Journal of Biomechanics 79 (2018) 212–217

Contents lists available at ScienceDirect

Journal of Biomechanics

journal homepage: www.elsevier.com/locate/jbiomech
www.JBiomech.com

Short communication

Automated, accurate, and three-dimensional method for calculating sagittal slope of the tibial plateau

Mark J. Amirtharaj [a], Brendan M. Hardy [a], Robert N. Kent III [a], Danyal H. Nawabi [b], Thomas L. Wickiewicz [b], Andrew D. Pearle [b], Carl W. Imhauser [a,*]

[a] Department of Biomechanics, Hospital for Special Surgery, Weill Cornell Medicine of Cornell University, 535 E 70th St, New York, NY 10021, USA
[b] Department of Orthopedic Surgery, Hospital for Special Surgery, Weill Cornell Medicine of Cornell University, 535 E 70th St, New York, NY 10021, USA

ARTICLE INFO

Article history:
Accepted 31 July 2018

Keywords:
Algorithm
Tibia
Slope
Sagittal
Lateral plateau
Anterior cruciate ligament
Noncontact
Rupture

ABSTRACT

Increased posterior-inferior directed slope of the subchondral bone of the lateral tibial plateau is a risk factor for noncontact rupture of the anterior cruciate ligament (ACL). Previous measures of lateral tibial slope, however, vary from study to study and often lack documentation of their accuracy. These factors impede identifying the magnitude of lateral tibial slope that increases risk of noncontact ACL rupture. Therefore, we developed and evaluated a new method that (1) requires minimal user input; (2) employs 3D renderings of the tibia that are referenced to a 3D anatomic coordinate system; and (3) is precise, reliable, and accurate. The user first isolated the proximal tibia from computed tomography (CT) scans. Then, the algorithm placed the proximal tibia in an automatically generated tibial coordinate system. Next, it identified points along the rim of subchondral bone around the lateral tibial plateau, iteratively fit a plane to this rim of points, and, finally, referenced the plane to the tibial coordinate system. Precision and reliability of the lateral slope measurements were respectively assessed via standard deviation and intra- and inter-class correlation coefficients using CT scans of three cadaveric tibia. Accuracy was quantified by comparing changes in lateral tibial slope calculated by our algorithm to predefined *in silico* changes in slope. Precision, reliability, and accuracy were $\leq 0.18°$, ≥ 0.998, and $\leq 0.13°$, respectively. We will use our novel method to better understand the relationship between lateral tibial slope and knee biomechanics towards preventing ACL rupture and improving its treatment.

1. Introduction

Rupture of the anterior cruciate ligament (ACL) is a common, costly, and debilitating knee injury (Brophy et al., 2009; Griffin et al., 2006; Lohmander et al., 2007). Therefore, researchers have sought to identify factors that heighten risk for this lesion. One such factor is increased posterior-inferior directed slope of the lateral tibial plateau, which elevates risk of not only noncontact ACL rupture (Beynnon et al., 2014; Dare et al., 2015), but revision surgery (Ahmed et al., 2017), and instability in the setting of ACL deficiency (Rahnemai-Azar et al., 2017; Song et al., 2016).

Planar methods for measuring sagittal slope of the lateral tibial plateau yield variable results from study to study (Bisson and Gurske-DePerio, 2010; Wordeman et al., 2012), which impedes identifying the magnitude of tibial slope that increases risk of noncontact ACL rupture. Previous techniques have utilized lateral radiography or a single, sagittal slice from a magnetic resonance imaging (MRI) scan (Hashemi et al., 2010; Hudek et al., 2009). Although these two-dimensional (2D) methods are easy to implement, they have limitations. Specifically, sagittal slope of the medial and lateral compartments are difficult to distinguish on lateral radiographs (Hashemi et al., 2010; Hudek et al., 2009; Kessler et al., 2003). In addition, planar measures of slope using manually identified reference points exhibit variations ranging from ±1.4° to ±4.8° (Caylor et al., 2001; Hudek et al., 2009). Finally, inconsistent alignment of the tibia relative to the imaging device influences planar slope measurements by 3.1° to 14° (Kessler et al., 2003; Utzschneider et al., 2011).

Sagittal tibial slope has also been measured using 3D reconstructions of the proximal tibia from MRI. Simon et al. fit a plane to the medial and lateral subchondral surfaces of the tibial plateau including the tibial spine (Simon et al., 2010). Interestingly, the tibial spine exhibits high interpersonal variability (medial tibial spine volume measured 326 ± 171 mm^3 across 88 subjects), which may increase uncertainity of the slope measurement (Sturnick et al.,

* Corresponding author at: 535 E 70th St, New York, NY 10021, USA.
E-mail address: imhauserc@hss.edu (C.W. Imhauser).

https://doi.org/10.1016/j.jbiomech.2018.07.047
0021-9290/© 2018 Elsevier Ltd. All rights reserved.

2014). Amerinatanzi et al. calculated tibial slope from a 3D Gaussian curvature analysis that required extensive user input, which could be another source of variability (Amerinatanzi et al., 2017).

Identifying relationships between tibial slope and biomechanical function of the knee is important to understand why certain individuals are more susceptible to ACL rupture. Thus, we aimed to advance the ability to measure sagittal slope of the tibial plateau by describing and evaluating a method that (1) requires minimal user input; (2) uses 3D renderings of the tibia; and (3) is precise, reliable, and accurate.

2. Methods

2.1. Algorithm Description

The algorithm to quantify tibial slope consists of five steps: (1) generating a point cloud of the proximal tibia obtained from 3D image data; (2) defining an anatomic coordinate system for the proximal tibia; (3) identifying the lateral rim of the tibial plateau (RTP); (4) iteratively fitting a plane to the lateral RTP; and (5) computing the sagittal slope of the lateral RTP relative to the anatomic coordinate system. Steps two through five are automated via custom code developed using MATLAB (v2016b, Natick, MA).

(1) Generating the 3D tibial point cloud

Computed tomography (CT) scans (Biograph, Siemens Inc., Munich, Germany) of three cadaveric knee specimens free of joint degeneration, deformity, or injury were obtained (3 male; ages 21, 21, and 43). The specimens were all young and without injury, and, therefore, are representative of those suffering first-time, noncontact ACL rupture. Each specimen was scanned axially with 0.6 mm slice thickness and $0.5 \times 0.5\ mm^2$ in-plane pixel dimensions (settings: 140 kV and 140 mA). Each tibia was segmented using grey value thresholding via Mimics software (Materialise Inc., Leuven, Belgium); then, the 3D spatial coordinates (or points) describing the tibial surface were exported in Stereolithography format (Fig. 1A). These data were subsequently imported into Geomagic software (3D Systems Inc., Rock Hill, SC), smoothed, and remeshed to a uniform point distribution (40% smoothing, 0.5 mm target edge length). Next, the tibial geometry was rotated to approximately align its long axis with the global Z-axis (Fig. 1B). Then, the proximal 15 cm of the tibia starting from the peak of the medial tibial spine was isolated, which corresponded to about 40% of the total length of the tibia (Fig. 1C). A tibial length of 15 cm is typically available in cadaver studies of knee joint biomechanics (Imhauser et al., 2013). This length also includes the tibial tubercle, whose geometry and location may vary from person to person (Brzobohatá et al., 2016). Finally, the rest of the tibial geometry was deleted and the proximal tibia was saved as an ASC vertex file.

(2) Defining the tibial coordinate system

The anatomical coordinate system for the proximal tibial geometry, or tibial coordinate system, was defined using a previously published method (Kai et al., 2014). First, the long axis (Z-axis) was computed via principle component analysis (PCA) (Fig. 2A). PCA identified the direction of most variance in the point data describing the proximal tibia (Pearson, 1901); this direction aligned with the tibial long axis. Next, the medial-lateral (ML) and anterior-posterior (AP) axes of the tibial coordinate system were defined using the most contoured ellipse, which has the largest sum of major and minor axes lengths (Fig. 2B, C). The most contoured ellipse was identified by successively fitting an ellipse to point data located within transverse slices perpendicular to the long axis of the tibia in 0.3 mm increments. The major and minor axes of the most contoured ellipse were set as the respective ML (Y-axis) and AP (X-axis) axes of the tibial coordinate system (Fig. 2C, D) (Bobrowitsch et al., 2007); the center of this ellipse was defined as the origin of the tibial coordinate system.

(3) Identifying the lateral rim of the tibial plateau

The lateral tibial plateau was isolated by eliminating all points >20 mm inferior and >10 mm medial to the peak of the medial tibial spine. This range isolated the set of points describing the surface of the lateral plateau and a portion of the proximal tibial metaphysis. Then, this set of points was used to identify the periphery, or rim, of the lateral plateau. Specifically, the points on the lateral RTP were defined to correspond to the location of maximum curvature when traversing radially over the edge of the tibia and inferiorly down the tibial metaphysis (Fig. 3). To identify the points comprising the lateral RTP, first, a point located centrally on the lateral plateau provided a reference for our algorithm. This central point was specified to be at the peak of the medial tibial spine in the AP direction, 25% of the length of the major axis of the most contoured ellipse in the ML direction, and at the origin of the anatomic coordinate system in the superior-inferior (SI) direction (Fig. 3). These

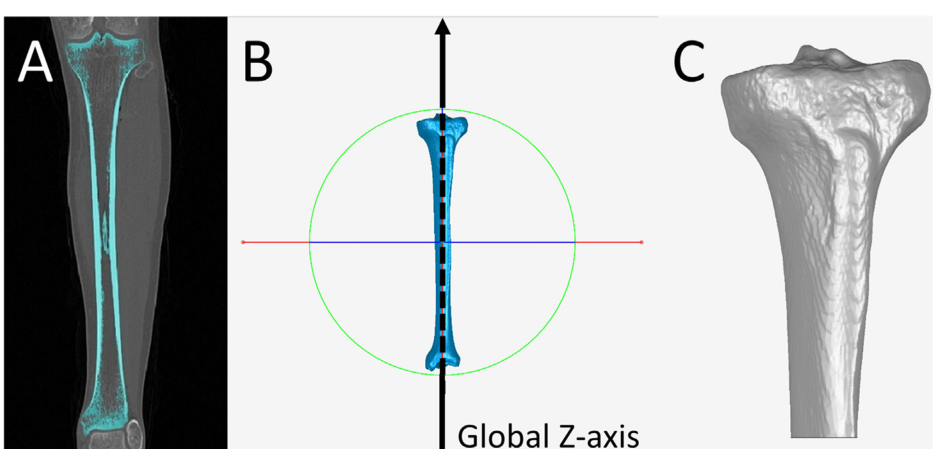

Fig. 1. Overview of the steps used to generate the point cloud describing the proximal tibial geometry. The steps were (A) masking each 2D slice of the tibial geometry from a CT scan as outlined in blue and then developing a 3D rendering; (B) approximately aligning the long axis of the 3D tibial geometry with the global Z-axis; and (C) isolating the proximal 15 cm of the tibial geometry. (For interpretation of the references to colour in this figure legend, the reader is referred to the web version of this article.)

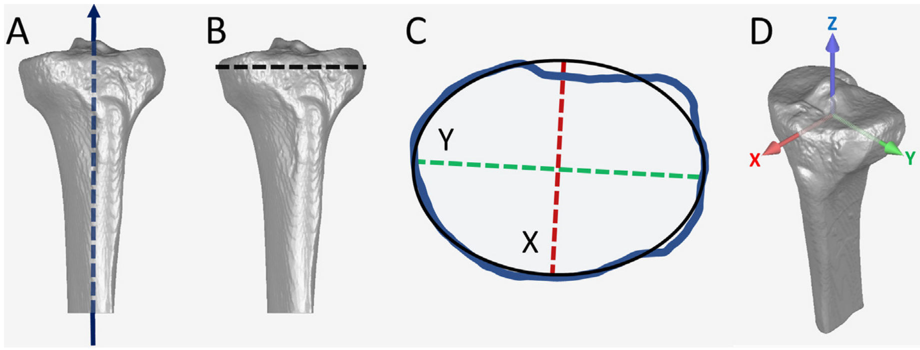

Fig. 2. Anatomical coordinate system for the proximal tibia. The anatomical coordinate system for the proximal tibia was generated using principal component analysis. (A) The long axis (dashed, blue line), or Z-axis, of the tibia is shown on an anterior view. (B) ML and AP axes were identified from a transverse plane (dashed, black line) that was perpendicular to the Z-axis. (C) This transverse plane contained the cross-section of the tibial geometry (blue) that, after fitting with an ellipse (black), was the most contoured. ML (green, Y) and AP (red, X) axes were the respective major and minor axes of the most contoured ellipse. (D) The X, Y, and Z axes, together, defined the coordinate system for the proximal tibia. (For interpretation of the references to colour in this figure legend, the reader is referred to the web version of this article.)

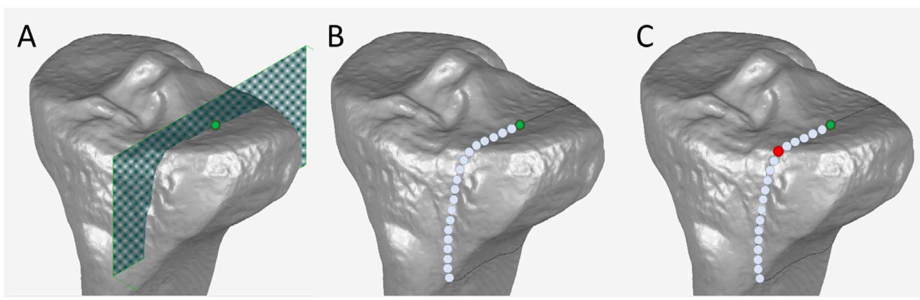

Fig. 3. Summary of the method used to identify a point of maximum curvature on the lateral rim of the tibial plateau. (A) First, a plane coincident with a central point on the lateral plateau (green circle) and parallel to the long axis (Z-axis) of the tibia was defined. (B) Then, the points on the surface of the tibial geometry (grey circles) within ±2 mm of this plane were isolated. (C) Next, the point of maximum curvature was identified from this subset of points (red circle) using an objective algorithm. (For interpretation of the references to colour in this figure legend, the reader is referred to the web version of this article.)

values yielded a point that was located centrally on the lateral plateau via visual inspection. A sagittal plane containing the plateau center was then created (Fig. 3A). All points comprising the lateral tibial plateau that were within 0.2 mm of either side of this plane were selected (Fig. 3B). Next, the point of maximum curvature was identified within this subset of points using an objective algorithm (Satopää et al., 2011) (Fig. 3C). This objective algorithm first calculated a vector between the endpoints of the data set; then, the point of maximum curvature corresponded to the point that formed the longest perpendicular to this vector. Subsequently, the initial, sagittal plane was rotated incrementally around an axis that coincided with the plateau center and was parallel with the Z-axis (Fig. 4). The plane was rotated relative to this axis in increments of 3° (0.0167π) from an initial angle of 0.9π to a final angle of 2.1π (Fig. 4A). The values for each parameter (rotation increment, initial angle, and final angle) were selected based on sensitivity analyses indicating that they provided the most accurate measure of slope (Supplementary Material). At each rotation increment, the method described above was repeated (Fig. 4B); a total of 72 points represented the lateral RTP.

Supplementary data associated with this article can be found, in the online version, at https://doi.org/10.1016/j.jbiomech.2018.07.047.

(4) Iteratively fitting a plane to the lateral rim of the tibial plateau

It was observed that the point of maximum curvature varied as a function of the magnitude of sagittal tibial slope, which influenced our slope measurement. To account for this source of variability, the orientation of the tibial plateau was standardized relative to the tibial coordinate system. To do this, a plane was first fit to the points outlining the lateral RTP using a least squares algorithm (Fig. 5). Then, the orientation of the normal vector of the best-fit plane to the lateral RTP was determined relative to the tibial long axis (Z-axis). Next, the proximal tibial geometry was rotated such that the best-fit plane's normal vector was parallel to the tibial long axis. This rotation realigned the tibial plateau to be more parallel with the transverse (X-Y) plane of the tibial coordinate system. Then, the points representing the lateral RTP were again determined with the reoriented tibia as described in step 3 above. The new lateral RTP points were then rotated back to the original anatomic orientation using the inverse of the previously described rotation matrix. A new plane was then fit to the most recently calculated and rotated points along the RTP and, finally, the angle between this new plane and the AP axis of the tibial coordinate system, i.e. the sagittal slope, was computed using the dot product operation. After ten iterations, the sagittal slope measurement varied by $\leq \pm 0.02°$ for all three tibial geometries that were evaluated (Fig. 6).

(5) Computing sagittal slope

The sagittal slope of the lateral tibial plateau was reported as the average value obtained from the 10th iteration to the 20th iteration of the plane fitting algorithm (described in step 4). A positive value indicated a posterior-inferior directed slope and a negative value indicated a posterior-superior directed slope relative to the AP axis of the tibial coordinate system.

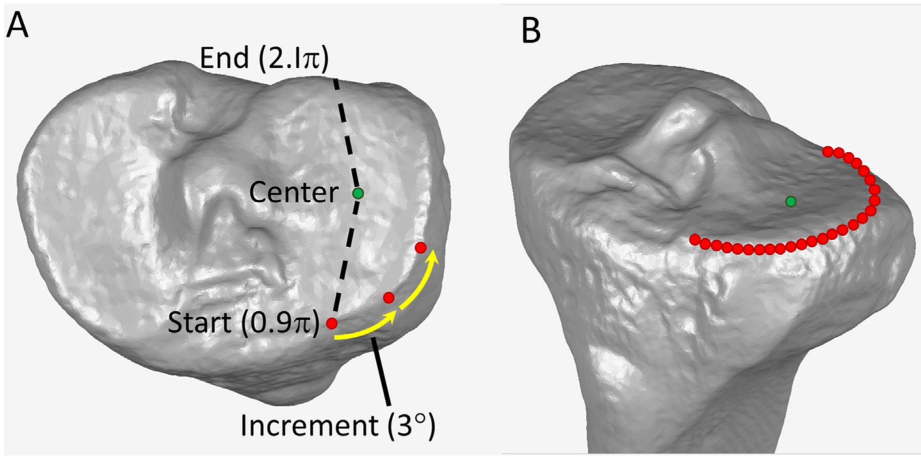

Fig. 4. Identifying the points of maximum curvature along the lateral rim of the tibial plateau. (A) The points of maximum curvature (red dots) were identified by rotating a plane (black, dashed line) that was coincident with the center of the lateral plateau (green circle labelled Center) and parallel to the long axis (Z-axis) of the tibia. The plane was rotated from the initial (Start) to the final (End) angles, which were defined relative to the AP axis of the tibial coordinate system with the anterior and posterior directions corresponding to π and 2π, respectively. The Start and End angles were located at 0.9π (162°) and 2.1π (378°), respectively, and the plane was rotated in increments of 0.0167π (3°). (B) Retrieving one point of maximum curvature per increment produced a set of 72 points (red circles) along the lateral rim of the tibial plateau (all 72 points are not shown). (For interpretation of the references to colour in this figure legend, the reader is referred to the web version of this article.)

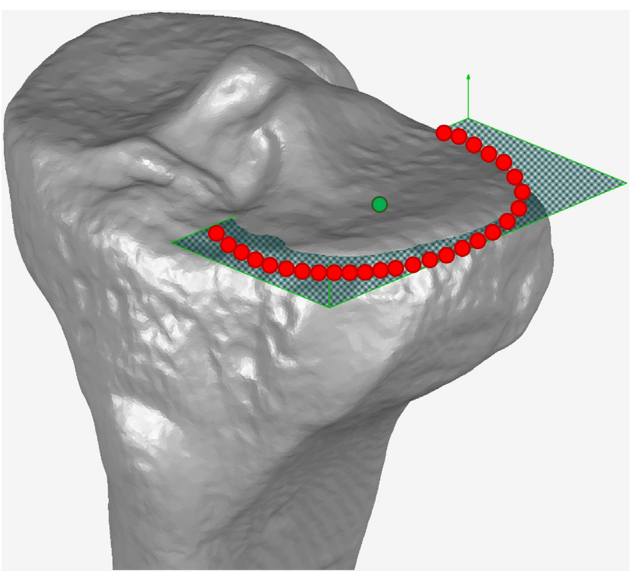

Fig. 5. Fitting a plane to points outlining the lateral rim of the tibial plateau (RTP). A plane (checkered pattern) was fit to the points of maximum curvature along the lateral RTP (red circles). The angle of the best fit plane with respect to the AP axis of the tibial coordinate system was computed. A positive angle indicated a posterior-inferior directed sagittal slope of the lateral tibial plateau. (For interpretation of the references to colour in this figure legend, the reader is referred to the web version of this article.)

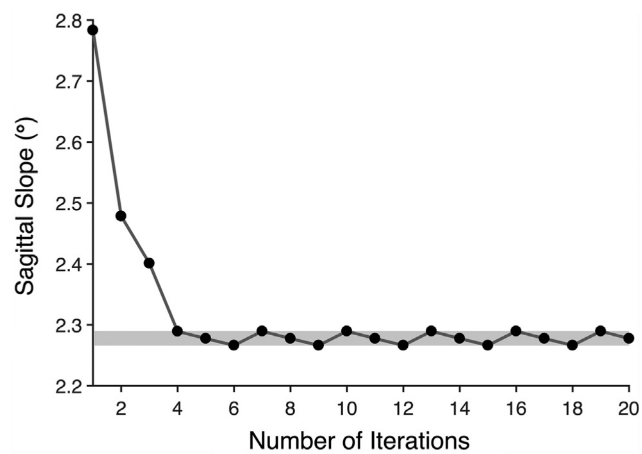

Fig. 6. Representative graph illustrating how the measure of sagittal slope of the lateral tibial plateau varied by $\leq\pm0.02°$ from the 10th iteration to the 20th iteration of the algorithm as indicated by the grey band.

2.2. Experimental design

2.2.1. Accuracy assessment

To quantify the accuracy of our algorithm, the sagittal slope of the three tibial geometries was altered *in silico* to establish a gold standard. Specifically, virtual osteotomies of each tibial geometry were made using Geomagic software. First, with the tibial geometry oriented in its anatomic coordinate system, a transverse cut was made 30 mm inferior to the peak of the medial tibial spine. The 30 mm distance ensured that all virtual, *in silico* cuts cleared (i.e., did not intersect) the tibial plateau. Next, a second cut was made by rotating a transverse plane around the ML axis of the tibial coordinate system in eight increments: −9°, −6°, −3°, −1°, +1°, +3°, +6°, and +9°. The slope increments were chosen to span the range of slope values reported in the literature (Beynnon et al., 2014; Dare et al., 2015; Rahnemai-Azar et al., 2016; Wordeman et al., 2012). For each increment, the section of tibia in between the transverse cut and the rotated plane was removed; then, the proximal and distal tibial segments were merged (Fig. 7). The sagittal slope of the lateral plateau for each version of each tibial geometry (with and without the virtual osteotomies) was then calculated using our algorithm. To quantify the accuracy of our algorithm, first, the change in slope for each virtual osteotomy relative to that of the original tibial geometry was determined. Then, the difference between the predefined change in slope and the change determined using our algorithm was calculated.

2.2.2. Precision and reliability assessment

Precision was reported via standard deviations of the slope measurements. To assess inter-observer reliability, which reflects variations in the segmentation of the tibial geometry, three individuals independently segmented each tibia. To assess intra-observer reliability, one individual segmented each tibia three times, one week apart. Slope was calculated for all of the segmen-

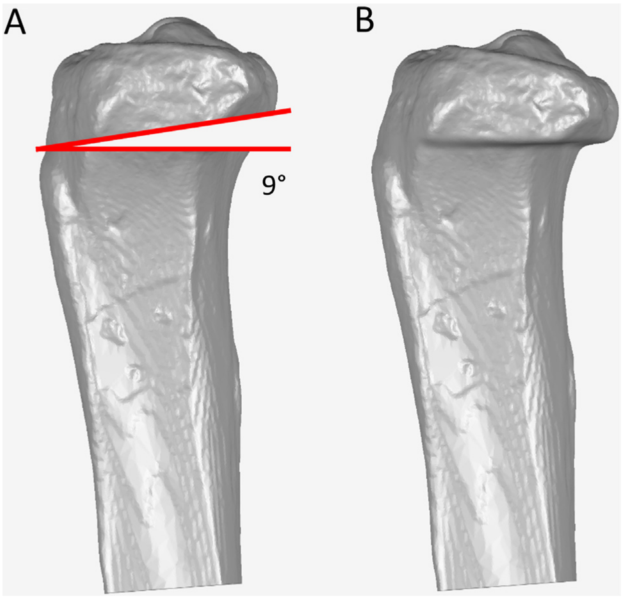

Fig. 7. Virtual osteotomy of the tibial geometry to assess the accuracy of our algorithm to calculate sagittal slope of the lateral tibial plateau. (A) Lateral views of a 3D reconstructed proximal tibial geometry obtained from computed tomography after removing a 9° posterior wedge and (B) after merging the remaining proximal and distal portions of the tibia.

tations. Inter- and intra-observer reliabilities were quantified using inter- and intra-class correlation coefficients (ICC), respectively.

3. Results

In terms of accuracy, the changes in sagittal slope for the three tibial geometries as measured using our algorithm differed from the predefined change in slope from −0.10° to 0.13° (Table 1).

In terms of precision, the largest standard deviations for the intra- and inter-observer measurements for each tibial geometry were ±0.03° and ±0.18°, respectively (Tables 2, 3). The ICCs for intra- and inter-observer reliability were 0.999 and 0.998, respectively.

4. Discussion

An automated, accurate, precise, and reliable method of measuring sagittal slope of the lateral tibial plateau using geometries obtained from CT imaging was developed. The accuracy of our method (0.13° maximum error, Table 1) was 19 times greater than the difference in sagittal slope between cases and controls (~2.5°) that increases risk of noncontact ACL injury (Beynnon et al., 2014; Dare et al., 2015; Rahnemai-Azar et al., 2016). Altogether, the algorithm will be useful for identifying relationships between tibial slope and biomechanical function of the knee joint.

Table 1
Accuracy assessment comparing measured changes in tibial slope (Δ slope) and predefined, *in silico* changes in tibial slope for three tibial geometries (Tibias 1, 2, and 3).

Predefined Δ slope (°)	Measured Δ slope (°) Tibia 1	Measured Δ slope (°) Tibia 2	Measured Δ slope (°) Tibia 3
−9.00	−8.88	−8.88	−8.92
−6.00	−5.87	−5.95	−5.99
−3.00	−2.91	−2.94	−2.96
−1.00	−0.99	−1.10	−0.90
1.00	1.04	1.00	1.10
3.00	3.01	3.08	3.01
6.00	5.93	6.10	6.07
9.00	8.93	9.02	9.07

Table 2
Intra-observer slope measurements made by a single examiner three times for each tibial geometry (Tibias 1, 2, and 3).

Measurement Trial	Tibia 1 (°)	Tibia 2 (°)	Tibia 3 (°)
1	2.28	−3.16	−0.05
2	2.26	−3.11	−0.03
3	2.26	−3.14	−0.01
Average ± Std. Dev.	2.27 ± 0.01	3.14 ± 0.03	−0.03 ± 0.02

Table 3
Inter-observer slope measurements made by three independent examiners (A, B, C) for each tibial geometry (Tibias 1, 2, and 3).

Examiner	Tibia 1 (°)	Tibia 2 (°)	Tibia 3 (°)
A	2.28	−3.16	−0.05
B	2.26	−2.81	0.04
C	2.43	−3.04	0.01
Average ± Std. Dev.	2.32 ± 0.09	−3.00 ± 0.18	0.00 ± 0.05

Our method has additional strengths. First, it requires minimal user decision making (besides segmenting the tibial geometry) to select reference axes and anatomic landmarks. Second, it is independent of tibial alignment within the scanner. These main strengths enable lateral slope measurements that are more reliable (Tables 2, 3) than previous methods (ICCs of 0.998 vs 0.76) (Dare et al., 2015). Our method also utilizes about 35 times more points than those that rely solely on an anterior and a posterior point on the tibial plateau (Dejour and Bonnin, 1994; Hashemi et al., 2010; Hudek et al., 2009). Thus, it is less sensitive to small variations in individual points. Our method is also independent of the tibial spine, which has large geometric variability (Sturnick et al., 2014). Finally, previous studies assessed accuracy by comparing to gold standards that were limited including long film, 2D radiographs (Faschingbauer et al., 2014) and digital goniometry on cadaveric tibias (Utzschneider et al., 2011). In contrast, we exactly changed the sagittal slope of the tibial plateau *in silico* and measured how accurately our method detected these virtual changes.

This study has limitations. First, tibial geometries were obtained from CT, which is not the clinical standard of care. Computed tomography, however, is more appropriate for our *in vitro* biomechanical research because radiation exposure is not a concern and because it provides excellent contrast of the bone to facilitate segmentation. Our method could also be utilized with MRI, which is more commonly used in the clinic; before doing so, its accuracy and reliability should be documented and compared to other techniques (Hashemi et al., 2010; Hudek et al., 2009). Second, our method computes the long axis of the tibial coordinate system from the proximal 15 cm of the tibia. This length is typically available for *in vitro* biomechanical studies but may not be captured on clinical scans. Nevertheless, sagittal slope has been measured using shorter tibial lengths of about 7 cm (Beynnon et al., 2014).

In conclusion, we have developed an automated, accurate, precise, and reliable method to calculate posterior-inferior directed slope of the lateral tibial plateau from CT scans. This method will be useful to identify relationships between this critical feature of tibial geometry and knee biomechanics towards preventing ACL rupture and improving its treatment.

Acknowledgements

This investigation was supported by the Clark and Kirby Foundations, the Surgeon in Chief Fund at Hospital for Special Surgery, and the Gosnell Family.

Conflict of interest statement

The following statement is in reference to the enclosed manuscript entitled "Automated, Accurate, and Three-dimensional Method for Calculating Sagittal Slope of the Tibial Plateau." None of the authors has any financial or personal relationships with other people or organizations that could inappropriately influence or bias this work.

References

Ahmed, I., Salmon, L., Roe, J., Pinczewski, L., 2017. The long-term clinical and radiological outcomes in patients who suffer recurrent injuries to the anterior cruciate ligament after reconstruction. Bone Joint J. 99-B, 337–343.

Amerinatanzi, A., Summers, R.K., Ahmadi, K., Goel, V.K., Hewett, T.E., Nyman, E., 2017. Automated measurement of patient-specific tibial slopes from MRI. Bioengineering (Basel) 4.

Beynnon, B.D., Hall, J.S., Sturnick, D.R., Desarno, M.J., Gardner-Morse, M., Tourville, T.W., Smith, H.C., Slauterbeck, J.R., Shultz, S.J., Johnson, R.J., Vacek, P.M., 2014. Increased slope of the lateral tibial plateau subchondral bone is associated with greater risk of noncontact ACL injury in females but not in males: a prospective cohort study with a nested, matched case-control analysis. Am. J. Sports Med. 42, 1039–1048.

Bisson, L.J., Gurske-DePerio, J., 2010. Axial and sagittal knee geometry as a risk factor for noncontact anterior cruciate ligament tear: a case-control study. Arthroscopy 26, 901–906.

Bobrowitsch, E., Imhauser, C., Graichen, H., Durselen, L., 2007. Evaluation of a 3D object registration method for analysis of humeral kinematics. J. Biomech. 40, 511–518.

Brophy, R.H., Wright, R.W., Matava, M.J., 2009. Cost analysis of converting from single-bundle to double-bundle anterior cruciate ligament reconstruction. Am. J. Sports Med. 37, 683–687.

Brzobohatá, H., Krajíček, V., Horák, Z., Velemínská, J., 2016. Sexual dimorphism of the human tibia through time: insights into shape variation using a surface-based approach. PloS One 15.

Caylor, K.B., Zumpano, C.A., Evans, L.M., Moore, R.W., 2001. Intra- and interobserver measurement variability of tibial plateau slope from lateral radiographs in dogs. J. Am. Anim. Hosp. Assoc. 37, 263–268.

Dare, D.M., Fabricant, P.D., McCarthy, M.M., Rebolledo, B.J., Green, D.W., Cordasco, F. A., Jones, K.J., 2015. Increased lateral tibial slope is a risk factor for pediatric anterior cruciate ligament injury: an MRI-based case-control study of 152 patients. Am. J. Sports Med. 43, 1632–1639.

Dejour, H., Bonnin, M., 1994. Tibial translation after anterior cruciate ligament rupture. Two radiological tests compared. J. Bone Joint Surg. Br. 76, 745–749.

Faschingbauer, M., Sgroi, M., Juchems, M., Reichel, H., Kappe, T., 2014. Can the tibial slope be measured on lateral knee radiographs? Knee Surg. Sports Traumatol. Arthrosc. 22, 3163–3167.

Griffin, L.Y., Albohm, M.J., Arendt, E.A., Bahr, R., Beynnon, B.D., Demaio, M., Dick, R. W., Engebretsen, L., Garrett Jr., W.E., Hannafin, J.A., Hewett, T.E., Huston, L.J., Ireland, M.L., Johnson, R.J., Lephart, S., Mandelbaum, B.R., Mann, B.J., Marks, P.H., Marshall, S.W., Myklebust, G., Noyes, F.R., Powers, C., Shields Jr., C., Shultz, S.J., Silvers, H., Slauterbeck, J., Taylor, D.C., Teitz, C.C., Wojtys, E.M., Yu, B., 2006. Understanding and preventing noncontact anterior cruciate ligament injuries: a review of the Hunt Valley II meeting, January 2005. Am. J. Sports Med. 34, 1512–1532.

Hashemi, J., Chandrashekar, N., Mansouri, H., Gill, B., Slauterbeck, J.R., Schutt Jr., R.C., Dabezies, E., Beynnon, B.D., 2010. Shallow medial tibial plateau and steep medial and lateral tibial slopes: new risk factors for anterior cruciate ligament injuries. Am. J. Sports Med. 38, 54–62.

Hudek, R., Schmutz, S., Regenfelder, F., Fuchs, B., Koch, P.P., 2009. Novel measurement technique of the tibial slope on conventional MRI. Clin. Orthop. Relat. Res. 467, 2066–2072.

Imhauser, C., Mauro, C., Choi, D., Rosenberg, E., Mathew, S., Nguyen, J., Ma, Y., Wickiewicz, T., 2013. Abnormal tibiofemoral contact stress and its association with altered kinematics after center-center anterior cruciate ligament reconstruction: an in vitro study. Am. J. Sports Med. 41, 815–825.

Kai, S., Sato, T., Koga, Y., Omori, G., Kobayashi, K., Sakamoto, M., Tanabe, Y., 2014. Automatic construction of an anatomical coordinate system for three-dimensional bone models of the lower extremities–pelvis, femur, and tibia. J. Biomech. 47, 1229–1233.

Kessler, M.A., Burkart, A., Martinek, V., Beer, A., Imhoff, A.B., 2003. Development of a 3-dimensional method to determine the tibial slope with multislice-CT. Z. Orthop. Ihre Grenzgeb 141, 143–147.

Lohmander, L.S., Englund, P.M., Dahl, L.L., Roos, E.M., 2007. The long-term consequence of anterior cruciate ligament and meniscus injuries: osteoarthritis. Am. J. Sports Med. 35, 1756–1769.

Pearson, K., 1901. On lines and planes of closest fit to systems of points in space. Philos. Mag., Series 6 (2), 559–572.

Rahnemai-Azar, A.A., Abebe, E.S., Johnson, P., Labrum, J., Fu, F.H., Irrgang, J.J., Samuelsson, K., Musahl, V., 2017. Increased lateral tibial slope predicts high-grade rotatory knee laxity pre-operatively in ACL reconstruction. Knee Surg. Sports Traumatol. Arthrosc. 25, 1170–1176.

Rahnemai-Azar, A.A., Yaseen, Z., van Eck, C.F., Irrgang, J.J., Fu, F.H., Musahl, V., 2016. Increased lateral tibial plateau slope predisposes male college football players to anterior cruciate ligament injury. J. Bone Joint Surg. Am. 98, 1001–1006.

Satopää, V., Albrecht, J., Irwin, D., Raghavan, B., 2011. Finding a "Kneedle" in a haystack: Detecting knee points in system behavior. In: 31st International Conference on Distributed Computing Systems Workshops, Minneapolis, pp. 166–117.

Simon, R.A., Everhart, J.S., Nagaraja, H.N., Chaudhari, A.M., 2010. A case-control study of anterior cruciate ligament volume, tibial plateau slopes and intercondylar notch dimensions in ACL-injured knees. J. Biomech. 43, 1702–1707.

Song, G.Y., Zhang, H., Wang, Q.Q., Zhang, J., Li, Y., Feng, H., 2016. Risk factors associated with grade 3 pivot shift after acute anterior cruciate ligament injuries. Am. J. Sports Med. 44, 362–369.

Sturnick, D.R., Argentieri, E.C., Vacek, P.M., DeSarno, M.J., Gardner-Morse, M.G., Tourville, T.W., Slauterbeck, J.R., Johnson, R.J., Shultz, S.J., Beynnon, B.D., 2014. A decreased volume of the medial tibial spine is associated with an increased risk of suffering an anterior cruciate ligament injury for males but not females. J. Orthop. Res. 32, 1451–1457.

Utzschneider, S., Goettinger, M., Weber, P., Horng, A., Glaser, C., Jansson, V., Muller, P.E., 2011. Development and validation of a new method for the radiologic measurement of the tibial slope. Knee Surg. Sports Traumatol. Arthrosc. 19, 1643–1648.

Wordeman, S.C., Quatman, C.E., Kaeding, C.C., Hewett, T.E., 2012. In vivo evidence for tibial plateau slope as a risk factor for anterior cruciate ligament injury: a systematic review and meta-analysis. Am. J. Sports Med. 40, 1673–1681.